International Journal of Nanomedicine

Dovepress
open access to scientific and medical research

Open Access Full Text Article

ORIGINAL RESEARCH

A dual-functional HER2 aptamer-conjugated, pH-activated mesoporous silica nanocarrier-based drug delivery system provides in vitro synergistic cytotoxicity in HER2-positive breast cancer cells

This article was published in the following Dove Press journal:
International Journal of Nanomedicine

Yinxing Shen[1,2]
Mengya Li[1]
Tianqi Liu[1]
Jing Liu[2]
Youhua Xie[2]
Junqi Zhang[2]
Shouhong Xu[1]
Honglai Liu[1]

[1]Key Laboratory for Advanced Materials, School of Chemistry and Molecular Engineering, East China University of Science and Technology, Shanghai 200237, People's Republic of China; [2]Key Laboratory of Medical Molecular Virology (MOE/NHC/CAMS), Department of Medical Microbiology and Parasitology, School of Basic Medical Sciences, Shanghai Medical College, Fudan University, Shanghai 200032, People's Republic of China

Correspondence: Junqi Zhang
Key Laboratory of Medical Molecular Virology (MOE/NHC/CAMS), Department of Medical Microbiology and Parasitology, School of Basic Medical Sciences, Shanghai Medical College, Fudan University, 138 Yixueyuan Road, Shanghai 200032, People's Republic of China
Tel +86 215 423 7972
Fax +86 215 423 7973
Email junqizhang@fudan.edu.cn

Shouhong Xu
Key Laboratory for Advanced Materials, School of Chemistry and Molecular Engineering, East China University of Science and Technology, 130 MeiLong Road, Shanghai 200237, People's Republic of China
Tel +86 216 425 2921
Fax +86 216 425 2921
Email xushouhong@ecust.edu.cn

Purpose: As well as functioning as a ligand that is selectively internalized by cells overexpressing human epidermal growth factor receptor-2 (HER2), HApt can exert cytotoxic effects by inducing cross-linking and subsequent translocation of HER2 to cytoplasmic vesicles, such downregulation of HER2 inhibits cell proliferation and induces apoptosis. We aimed to exploit the potential of HApt as both a targeting agent and antagonist to maximize the efficacy of mesoporous silica nanoparticle (MSN)-based drug release systems for HER2-positive breast cancer.

Materials and methods: We fabricated novel HApt aptamer-functionalized pH-sensitive β-cyclodextrin (β-CD)-capped doxorubicin (DOX)-loaded mesoporous silica nanoparticles (termed MSN-BM/CD-HApt@DOX) for targeted delivery and selective targeting of HER2-positive cells. MSN-functionalized benzimidazole (MSN-BM) was used to load and achieve pH stimuli-responsive release of the chemotherapeutic agent doxorubicin (DOX). β-cyclodextrin was introduced as a gatekeeper for encapsulated DOX and HApt as a selective HER2-targeting moiety and biotherapeutic agent.

Results: Physical and chemical characterizations (FT-IR, XRD, TEM and BET) confirmed successful construction of MSN-BM/CD-HApt@DOX nanoparticles. In vitro release assays verified pH-sensitive DOX release. MSN-BM/CD-HApt@DOX (relative DOX concentration, 3.6 μg/mL) underwent HER2-mediated endocytosis and was more cytotoxic to HER2-positive SKBR3 cells than HER2-negative MCF7 cells. MSN-BM/CD-HApt@DOX also exhibited better uptake and stronger growth inhibition in SKBR3 cells than the control MSN-BM/CD-NCApt@DOX functionalized with a scrambled nucleotide sequence on CD. Overall, intracellular delivery of DOX and the biotherapeutic agent HApt resulted in synergistic cytotoxic effects in HER2-positive cancer cells in comparison to either DOX or HApt alone.

Conclusion: MSN-BM/CD-HApt@DOX enables HER2-mediated targeting and biotherapeutic effects as well as pH-responsive DOX drug release, resulting in synergistic cytotoxic effects in HER2-overexpressing cells in vitro. This novel nanocarrier could potentially enable specific targeting to improve the efficacy of chemotherapy for HER2-positive cancer.

Keywords: mesoporous silica nanoparticle, pH-sensitive nanovalve, HER2 aptamer, synergistic cytotoxicity

Introduction

Conventional cancer chemotherapy encounters drastic limitations in terms of non-specific delivery of antitumor drugs and severe side-effects.[1,2] A variety of smart

drug-delivery systems with selective targeting and controlled release properties have been developed to minimize systemic cytotoxicity.[3] Mesoporous silica nanoparticles (MSN) have been widely used as drug release systems in recent decades due to their desirable properties, including good biocompatibility, high loading capacity and ease of functionalization.[4–6]

In order to avoid premature release in the blood circulation, MSNs are often equipped with a variety of stimuli-responsive nanovalves[7] such as inorganic nanoparticles,[8] polymers,[9–11] biomacromolecules[12-14] and supramolecular assemblies[15,16] to enable controlled drug release in response to external or internal stimuli. Supramolecular assemblies involved in host-guest interactions can function as nanovalves to effectively gate the pores of MSNs in a smart, simple manner. Supramolecular cyclodextrins (CD) are well-characterized, readily accessible host molecules that can be fixed on the surface of MSNs and participate in host-guest interactions with a variety of guest molecules.[17] When exposed to specific stimuli in the tumor microenvironment, such as changes in redox potential,[18] enzymatic activity,[14,19] temperature,[20] light[21,22] or acidic pH,[23,24] the interactions between CD and the guest molecules are disrupted, allowing the trapped drug to be released. For example, the aromatic amine guest molecule 1-methyl-1H-benzimidazole (BM) has a pKa of 5.67[25] and exhibits stable hydrophobic interactions with β-CD at physiological pH (7.4).[26,27] BM is protonated in the acidic tumor microenvironment, which opens the nanovalves and releases the trapped drug.

To enhance the accuracy of drug delivery to tumors, controlled drug-delivery systems have been functionalized with a variety of tumor-specific targeting ligands—such as aptamers,[28–30] peptides,[1,30–32] antibodies and growth factors[33]-to selectively target molecules and receptors that are overexpressed on the surface of tumor cells. Aptamers, single-stranded DNA or RNA oligonucleotides,[34,35] are a novel type of targeting agent that offer several advantages over other tumor-specific ligands. Aptamers bind their target of interest with high selectivity and affinity, are small and inexpensive to synthesize and have good chemical stability, low antigenic and immunogenic potential and excellent tissue penetration ability.[36–38] Although diverse aptamer-functionalized stimuli-responsive controlled release systems have been developed,[39–41] the potential of aptamers as both targeting and antagonistic agents to maximize the efficacy of drug delivery and cancer chemotherapy has not yet been fully exploited.

We previously demonstrated the aptamer HApt, which possesses both targeting and therapeutic capabilities,[42] specifically crosslinks with HER2 protein on the cell surface, which induces translocation of HER2 from the plasma membrane to cytoplasmic vesicles (mainly lysosomes) and subsequent digestion by proteases.[43] HApt-mediated targeting and downregulation of HER2 could inhibit cell proliferation and lead to cell death.[43] Therefore, HApt could potentially function as both a targeting ligand and biotherapeutic agent for smart drug delivery systems to improve the efficacy of chemotherapy for HER2-positive tumors. HER2 is expressed at higher levels (≈100-fold more) on the plasma membranes of various tumors,[42] including human ovarian, breast, lung and gastric cancer cells, than the corresponding normal cells.[44,45] Thus, inhibition of this transmembrane protein expression has been pursued as a target to improve the treatment of cancer.

Herein, we developed a pH-sensitive, tumor-targeted drug delivery system based on a HApt-functionalized pH-sensitive nanovalve (β-CD), named MSN-BM/CD-HApt @DOX. As illustrated in Scheme 1, DOX was loaded into the pores of BM surface-modified MSN, then the pores were capped with β-CD-SH through a host-guest interaction between β-CD and BM. The β-CD-SH was subsequently functionalized with HApt-SH through disulfide bonding. We hypothesized HApt would actively bind to HER2-overexpressing tumor cells, and thus reduce non-specific uptake by normal HER2-negative cells. Furthermore, after receptor-mediated endocytosis of the nanoparticles by HER2-positive tumor cells, β-CD would dissociate from the surface of the MSN in the acidic environment of cellular lysosomes/endosomes due to protonation of BM and disruption of the host-guest interaction, resulting in steady release of the encapsulated DOX from the pores of MSN in the cytoplasm of the target cells.

We report the novel nanocarrier MSN-BM/CD-HApt could efficiently encapsulate DOX and release the drug in a pH-dependent manner. Compared to MSN-BM/CD-NCApt@DOX functionalized with a scrambled nucleotide sequence on the CDs, MSN-BM/CD-HApt@DOX was more efficiently taken-up and exerted stronger cytotoxic effects in SKBR3 HER2-positive breast cancer cells. MSN-BM/CD-HApt@DOX was less cytotoxic towards MCF7 HER2-negative cells than SKBR3 HER2-positive cells. Therefore, MSN-BM/CD-HApt@DOX exerts a targeted synergies in HER2-positive cancer cells compared to either DOX or HApt monotherapy.

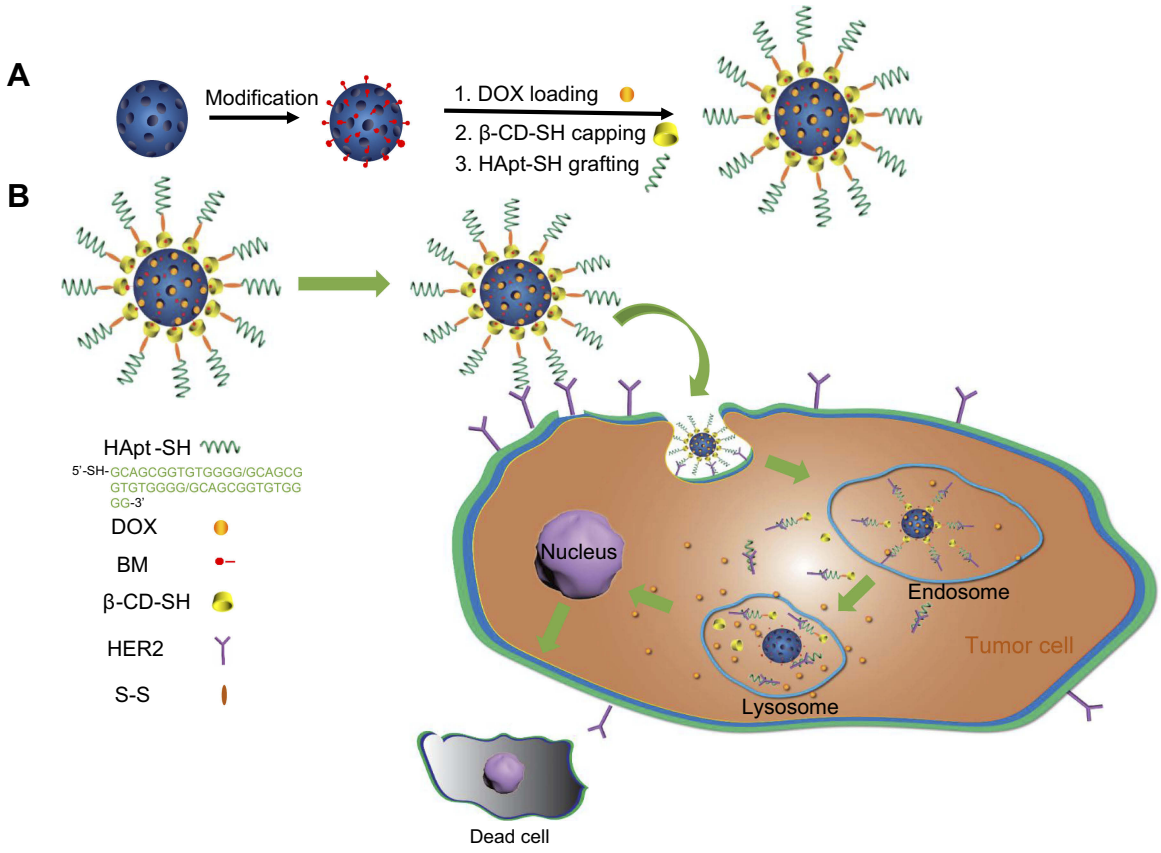

Scheme 1 Schematic representation of the structure of MSN-BM/CD-HApt@DOX (**A**) and the mechanism of HER2-mediated targeted combined therapy (**B**). **Abbreviations:** MSN, mesoporous silica nanoparticles; BM, benzimidazole; CD, β-cyclodextrin; HER2, human epidermal growth factor receptor-2; HApt, HER2 aptamer; DOX, doxorubicin.

Materials and methods

Materials

Cetyltriethylammonium bromide (CTAB), tetraethylorthosilicate (TEOS) and doxorubicin hydrochloride (DOX, 98%) were purchased from J&K Chemical Ltd. (Shanghai, China) and used as received. *N,N*'-dimethylformamide (99.8%), β-cyclodextrin (>97%), benzimidazole (98%), tetrabutylammonium iodide (98%), Hoechst 33,342 (≥97%), triethylamine (≥ 99%) and toluene (99.8%) were purchased from Sigma (St. Louis, MO, USA). Chloromethyltrimethoxysilane (>98%) was obtained from Tokyo Chemical Industry Co. Ltd. (Tokyo, Japan). Anti-HER2 aptamer (HApt, 5'-RS-S-C_6-GCA GCG GTG TGG GGG CAG CGG TGT GGG GGC AGC GGT GTG GGG-3') and HER2-negative control aptamer (NCApt, 5'-RS-S-C_6-ATT GCA CTT ACT ATA TTG CAC TTA CTA TAT TGC ACT TAC TAT-3') were commercially synthesized by Sangon Biotech Co., Ltd. (Shanghai, China).

Synthesis of mesoporous silica nanoparticles

Mesoporous silica nanoparticles (MSN) were synthesized according to published procedures.[27] Briefly, CTAB (1 g) was dissolved in H_2O (480 mL) and NaOH (2 M, 3.5 mL), heated to 80 °C, stirred for 30 min at 80 °C, then TEOS (4.8 mL) was added dropwise into the solution while stirring vigorously. The solution was kept at 80 °C for another 2 h. The white suspension was filtered, washed thoroughly with methanol, vacuum dried at 45 °C, and MSNs were obtained upon removal of the CTAB template by calcination at 550 °C for 6 h.

Modification of MSN with 1-methyl 1H-benzimidazole

As previously described,[23] MSN (100 mg) were washed and dispersed in anhydrous toluene, mixed with chloromethyltrimethoxysilane (15 μL), and refluxed for 12 h at 80 °C. The modified MSN were washed with toluene and

dimethylformamide (DMF) and dispersed in 8 mL of DMF. Tetrabutyammonium iodide (2 mg), 1-methyl 1*H*-benzimidazole (12 mg) and triethylamine (150 μL) were added to the solution, heated to 70 °C under N_2 for 24 h, and the product was thoroughly washed with DMF, methanol, and water.

Drug loading and capping

For drug loading, MSN-BM (100 mg) was dispersed in PBS buffer (pH 7.4, 1 mM, 20 mL), sonicated for 10 min, and DOX (2 mg/mL, 5 mL) was added. The mixture was stirred in the dark at room temperature for 24 h to ensure DOX was entrapped in the mesopores. The capping molecule β-CD-SH (400 mg) was added to the suspension and stirred for 12 h in a nitrogen atmosphere. The product was named MSN-BM/CD@DOX.

The disulfide bond on the anti-HER2 aptamer (HApt) was cleaved by adding 20 μL of 2.5 mM tris(2-carboxyethyl)phosphine (TCEP; Sigma-Aldrich) to 20 μL of 500 μM HApt solution for 30 min.[42] The resulting thiolated aptamer solution was added to the MSN-BM /CD@DOX suspension, and the mixture was stirred at room temperature for 24 h in air. The nanoparticles were collected by centrifugation, washed extensively with PBS to remove unloaded DOX, and the fluorescence of the supernatant was measured at an excitation wavelength of 480 nm, emission wavelength of 550 nm.

Drug-loading content (DLC) and drug-loading efficiency (DLE) were determined using equations (1) and (2):

DLC=(weight of drug loaded in MSN/weight of MSN)×100% (1)

DLE=(weight of drug loaded in MSN/weight of feed drug)×100% (2)

Control MSN-BM/CD-NCApt@DOX was prepared in a similar manner using the scrambled NCApt sequence instead of HApt.

Characterization

Transmission electron microscopy (TEM; JEM-1400; JEOL, Tokyo, Japan) was used to characterize the morphology of the prepared samples; ζ potential and size distribution were analyzed by dynamic light scattering (DLS; Zetasizer Nano ZS; Malvern Instruments, Malvern, UK). Fourier transform infrared (FT-IR) spectra were generated with a Nicolet Magna-IR 550 FTIR spectrometer in the range of 4000–400 cm^{-1}. Thermogravimetric analysis (TGA) was carried out on a Netzsch STA449F3 TG-DSC (TGA Instruments; Selb, Germany) in N_2 at a heating rate of 10 °C/min from 298 to 1073 K. Low-angle X-ray diffraction (XRD) patterns were obtained in a Bruker D8 Focus diffractometer using Cu Kα radiation at a scanning speed of 0.5°/min from 0.6 to 8°. Nitrogen adsorption-desorption isotherms were obtained on a volumetric adsorption analyzer ASAP 2020 (Micromeritics, Atlanta, GA, USA) at liquid nitrogen temperature (77.35 K) to measure pore size distribution and surface area.

Evaluation of pH-responsive drug release in vitro

To examine DOX release from MSN-BM/CD-HApt @DOX, fluorescence spectrophotometry (F-4500; Hitachi, Tokyo, Japan) was used to assess the fluorescence intensity of the supernatant at an excitation wavelength of 480 nm, emission wavelength of 550 nm. Briefly, 2 mg dried MSN-BM/CD-HApt@DOX powder was added in a glass vial containing 20 mL PBS (1 mmol/L, pH 4.5, 6.4 or 7.4) at 37 °C. At specific time intervals, 2 mL of the supernatant was taken out for analysis and then put back to keep the volume of release media constant. The DOX concentration was calculated using a fluorescence standard calibration curve (Figure S1).

Cumulative DOX release rate (%) was calculated using *w1/w2*× 100, where *w1* is the amount of DOX released from MSN-BM/CD-HApt@DOX at different time points and *w2* is the amount of DOX loaded in MSN-BM/CD-HApt@DOX.

Cell lines and culture

Human MCF7 and SKBR3 breast cancer cells and human 293T embryonic kidney cells were obtained from the American Type Culture Collection (Manassas, VA, USA). SKBR3 cells were maintained in McCoy's 5A medium (Thermo Fisher Scientific, Waltham, MA, USA) and HeLa cells and MCF7 cells were maintained in Dulbecco's Modified Eagle's Medium (DMEM; Thermo Fisher Scientific); both media were supplemented with 100 U/mL penicillin G/streptomycin sulfate and 10% (*v/v*) fetal bovine serum (FBS; Thermo Fisher Scientific) and all cells were cultured at 37 °C in a 5% CO_2 atmosphere.

Cell viability assays

Cells were seeded into collagen-coated 96-well plates (10^4 cells/well), incubated for 24 h, exposed to different concentrations of MSN-BM/CD-HApt, MSN-BM/CD-NCApt or MSN-BM/CD for 4 h, then the media was replaced by

fresh complete medium and incubated for another 20 h. Cell viability was measured using the Cell Counting Kit-8 (CCK-8; Dojindo, Kumamoto, Japan).

To assess HER2 receptor inhibition, SKBR3 cells were pretreated with free HApt (1 μM) for 30 min, and then incubated with MSN-BM/CD-HApt@DOX or MSN-BM /CD-NCApt@DOX containing different concentrations of DOX for 4 h, then cell viability assays were carried out as described above.

Cellular uptake assays

SKBR3 cells and MCF7 cells were seeded in 35mm glass bottom dish and allowed to attach overnight, then incubated with MSN-BM/CD-HApt@DOX or MSN-BM/CD-NCApt@DOX (DOX concentration, 3.6 μg/mL) for 4 h, followed the culture medium was removed, the cells were washed several times with PBS, and the nuclei were counterstained with Hoechst 33,342 (Sigma-Aldrich) for 10 min at room temperature. DOX fluorescence was examined by confocal microscopy (TCS SP8; Leica Microsystems, Wetzlar, Germany).

To assess HER2 receptor inhibition, SKBR3 cells were pretreated with free HApt (1 μM) for 30 min, and then incubated with MSN-BM/CD-HApt@DOX or MSN-BM /CD-NCApt@DOX (DOX concentration, 3.6 μg/mL) for 4 h, then treated as described above.

Flow cytometry

SKBR3 cells and MCF7 cells were plated in 24-well plates (10^6 cells/well), incubated for 24 h at 37 °C in a 5% CO_2 atmosphere, then 1 mL of DMEM containing MSN-BM /CD-HApt@DOX or MSN-BM/CD-NCApt@DOX (DOX concentration, 3.6 μg/mL) was added to each well, incubated for 4 h, then cells were washed twice with cold PBS, harvested and resuspended in PBS. Flow cytometry was performed on a fluorescence-activated cell sorting (FACS) Calibur flow cytometer (BD Biosciences, San Jose, CA, USA) and data were analyzed using FlowJo 7.6.1 (BD Biosciences).

Results and discussion

Preparation and characterization of MSN-BM/CD-HApt@DOX

As shown in the TEM images in Figure 1A, the monodispersed MSN had a uniform spherical morphology with well-ordered channel pores. After stepwise modification, the channels of the MSN became blurred and a gradually thicker shell appeared on the exterior of the MSN, indicating successful DOX loading, β-CD end-capping and HApt grafting. DLS analysis (Figure 1B) demonstrated the changes in the hydrodynamic diameters of the MSN during the fabrication process were consistent with the TEM observations. MSN-BM/CD-HApt@DOX (218.2±6.1nm, PDI: 0.263±0.014) had a larger hydrodynamic diameter than unmodified MSN (176.0± 4.2nm, PDI: 0.132 ±0.005) (Table S1), which may be due to the stepwise modification of MSN. The ζ potential of MSN was −23.5 ± 7.3 mV, while MSN-BM/CD-HApt@DOX was more negatively charged (−31.3 ± 1.4 mV) mainly due to modification with negatively charged HApt (Figure 1C). This negative surface charge may increase the circulation time of MSN-BM/CD-HApt@DOX in the blood.[46,47]

The structure of the MSN was further assessed by low-angle XRD (Figure 2A). The three well-defined diffraction peaks at (100), (110) and (200) indicated well-ordered hexagonal mesoporous MSN.[48] These peaks slightly decreased in intensity but were preserved during the fabrication process, suggesting the high structural stability and successful modification of the MSN.

FTIR and TGA were employed to confirm the surface modification of the MSN. The peaks at 3442cm^{-1} and 1629 cm^{-1} in Figure 2B indicate water physically absorbed to the surface of the MSN.[12] Compared to bare MSN, MSN-BM displayed two characteristic peaks at 1468cm^{-1} and 1394cm^{-1}, assigned to the C-N and C=N bonds of benzimidazole. These typical benzimidazole C-N and C=N signals disappeared when benzimidazole was embedded in the hydrophobic cavity of β-CD, suggesting the gatekeeper β-CD was immobilized onto MSN-BM via a host-guest interaction. Moreover, the presence of an amide I band at 1655 cm^{-1} and the C-N and C=N bands at 1420 cm^{-1} and 1391 cm^{-1} in MSN-BM/CD-HApt confirmed MSN-BM /CD was successfully modified with HApt. TGA revealed a gradual increase in weight loss after each surface functionalization step (Figure 2C). The weight loss values of blank MSNs, MSN-BM, MSN-BM/CD, and MSN-BM/CD-HApt were 11.1%, 17.98%, 21.91%, and 29.55%, respectively, further indicating each modification step was successful.

The BET nitrogen absorption-desorption isotherms and BJH pore size distributions of MSN, MSN-BM and MSN-BM/CD-HApt@DOX are shown in Figure 3. A typical type-IV isotherm curve was obtained, further confirming the well-defined mesoporous structure of the MSN (Figure 3A).[49] The stepwise functionalization process obviously decreased the BET surface area (S_{BET}), pore volume (V_P) and BJH pore

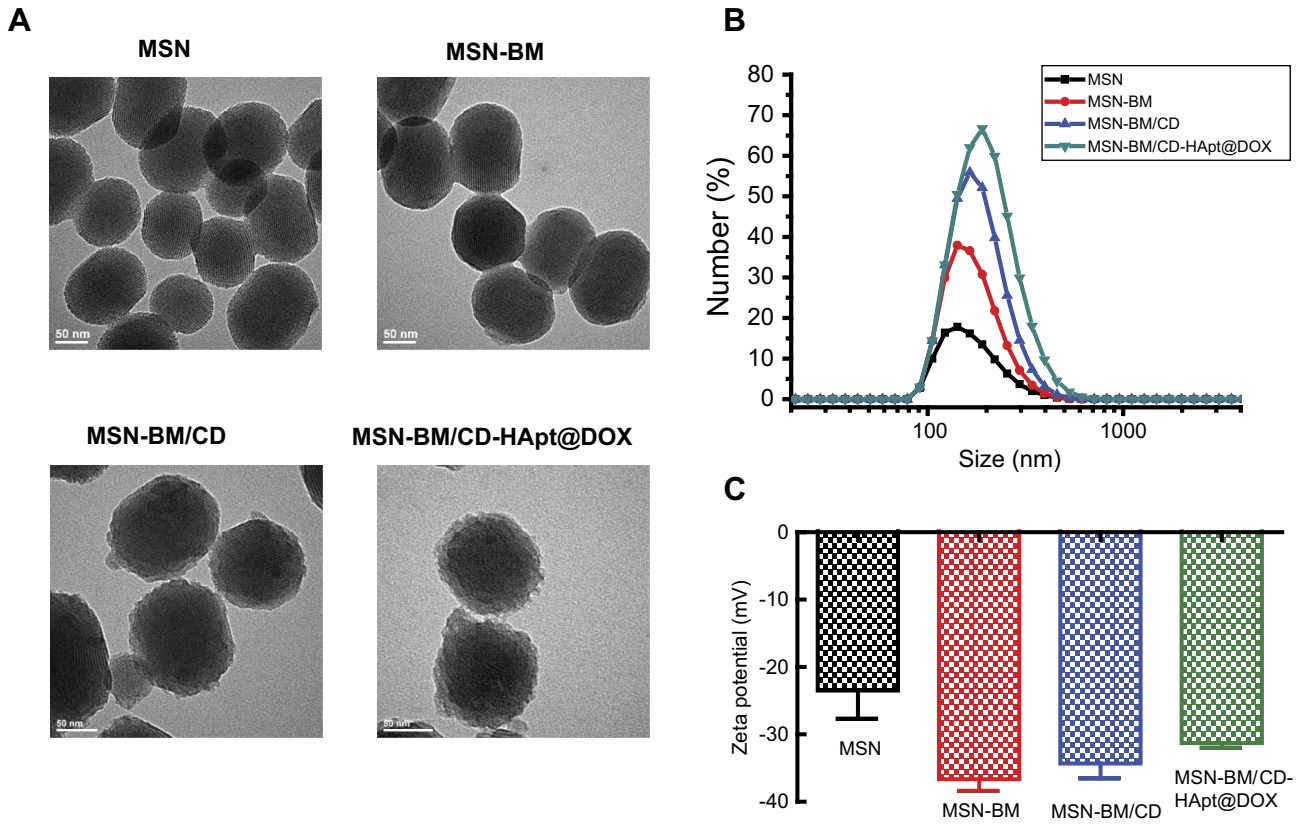

Figure 1 TEM images (**A**), size distribution (**B**) and ζ-potential values (**C**) of MSN, MSN-BM, MSN-BM/CD and MSN-BM/CD-HApt@DOX. Samples were dissolved in PBS (pH 7.4, 1 mM) for size and ζ-potential measurements. Data are mean ± SD (n=5).
Abbreviations: MSN, mesoporous silica nanoparticles; BM, benzimidazole; CD, β-cyclodextrin; HApt, aptamer; DOX, doxorubicin; PBS, phosphate buffered saline.

diameter (D_{BJH}) of the MSN (Table S1 and Figure 3A and B). The BET surface area of the nanoparticles decreased from 1007.9 m^2/g to 238.0 m^2/g and the pore volume decreased from 0.85 cm^3/g to 0.11 cm^3/g after DOX loading, β-CD capping and HApt grafting, indicating successful drug loading and complete blocking of the pores.

Effect of the MSN-BM synthetic pathway on drug loading and release capacity

To optimize the biofunction of the system for subsequent drug loading and release studies, we assessed two different MSN-BM synthetic pathways: removing the template before (Path I) or after (Path II) modification of the BM, which would determine whether BM exists in the porous MSN channels, as shown in Figure 4. The BET surface area and pore diameter were slightly lower for Path I (797.5 m^2/g, 2.23 nm) than Path II (811.5 m^2/g, 2.34 nm) (Table S3). However, Path I MSN-BM/CD-HApt@DOX had a much higher drug loading content (DLC: ~3.64 *wt%*) than Path II MSN-BM/CD-HApt @DOX (DLC: ~2.60 *wt%*) at pH 7.4 (Table S3). Overall, the drug storage capacity was higher in the presence of BM, due to the hydrophobic interaction between DOX and BM at pH 7.4.[25] However, the difference in DLC for the two synthetic pathways was not significant, indicating DOX could still be loaded into the MSNs in the absence of the hydrophobic interaction with BM in the porous channel.

Moreover, the drug release profiles (Figure 4) showed DOX was released from both Path I and Path II MSN-BM /CD-HApt@DOX in a pH-dependent manner. Removal of β-CD depends on protonation of BM in acidic conditions. In addition, the DOX release rates of both samples were similar: 19.93±3% and 29.52±2% for Path I nanoparticles (Figure 4A) and 18.92±4% nd 28.34±2% for Path II nanoparticles (Figure 4B) at pH 7.4 and 6.4, respectively. However, the release rate at pH 4.5 was higher for Path I nanoparticles (82.3±5%) (Figure 4A) than Path II nanoparticles (51.96±4%) (Figure 4B). The superior release capacity of Path I nanoparticles at low pH can be attributed to disruption of the hydrophobic interactions between DOX and BM in the porous MSN channels due to protonation of BM under acidic conditions.

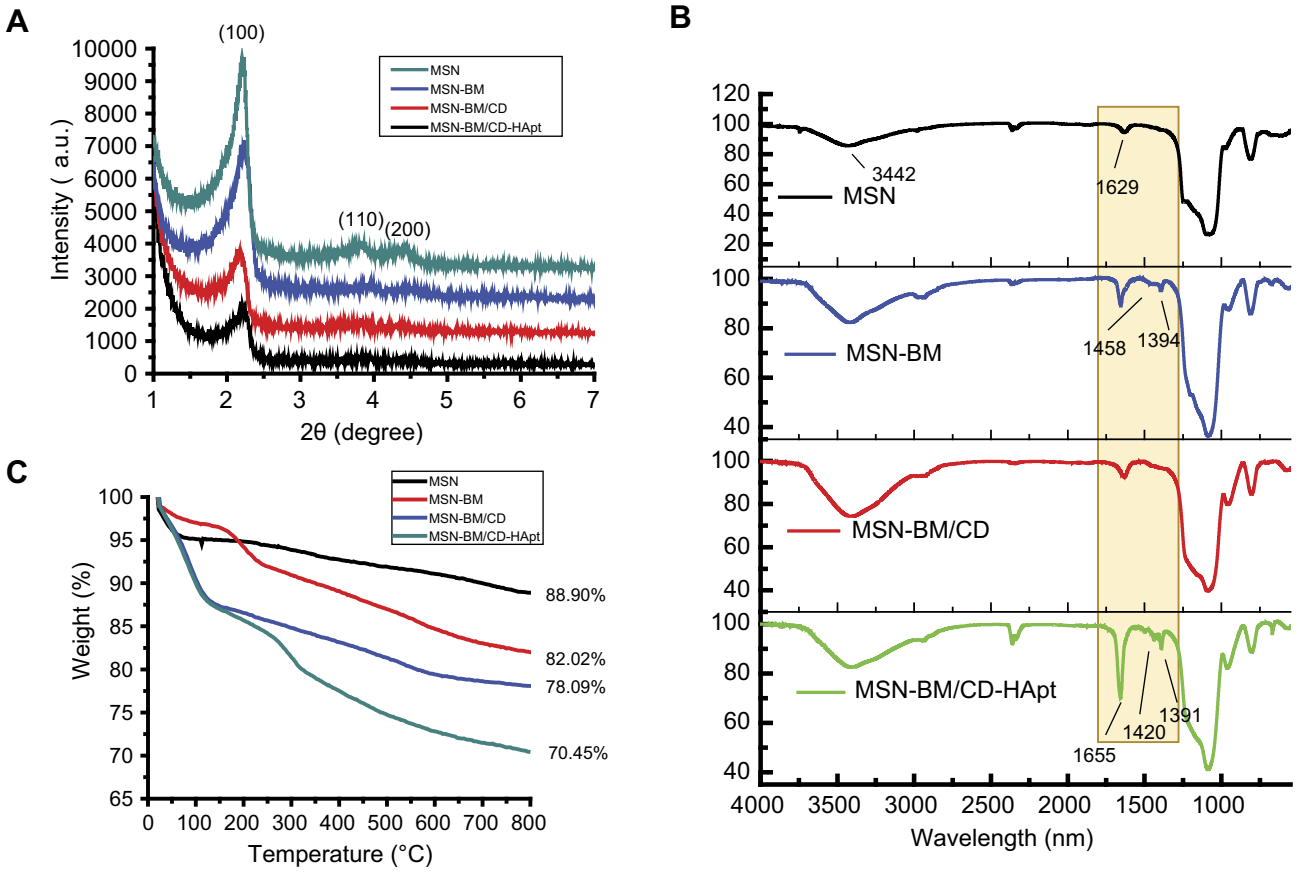

Figure 2 XRD analysis (**A**), FTIR spectra (**B**) and TGA curves (**C**) for MSN, MSN-BM, MSN-BM/CD and MSN-BM/CD-HApt.
Abbreviations: MSN, mesoporous silica nanoparticles; BM, benzimidazole; CD, β-cyclodextrin; HApt, aptamer; DOX, doxorubicin.

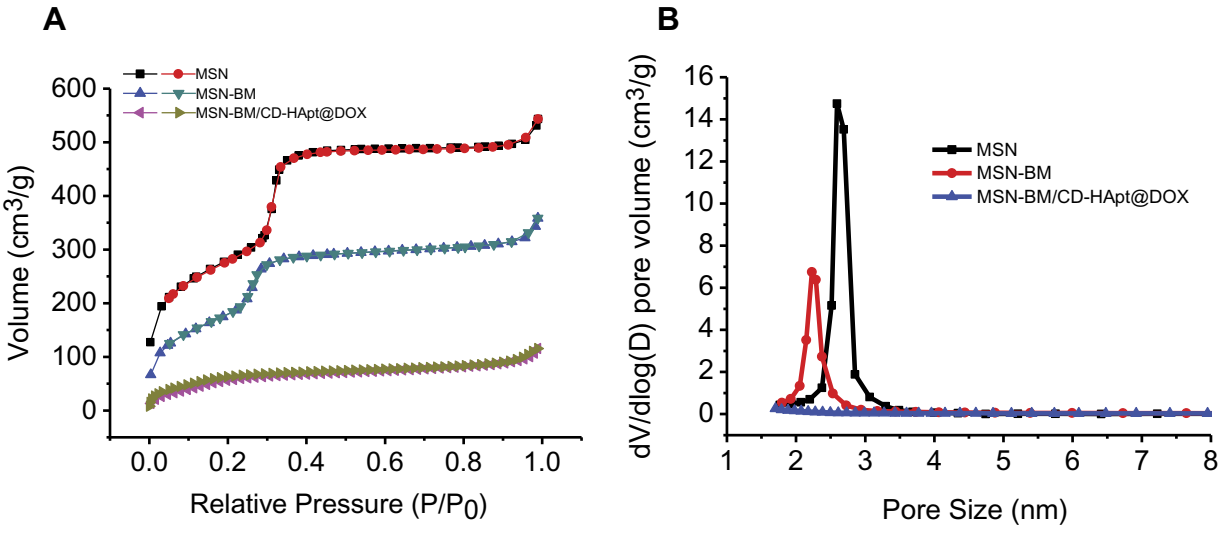

Figure 3 Brunauer–Emmett–Teller nitrogen adsorption/desorption isotherms (**A**) and Barrett–Joyner–Halenda pore size distributions (**B**) for MSN, MSN-BM and MSN-BM /CD-HApt@DOX.
Abbreviations: MSN, mesoporous silica nanoparticles; BM, benzimidazole; CD, β-cyclodextrin; HApt, aptamer; DOX, doxorubicin.

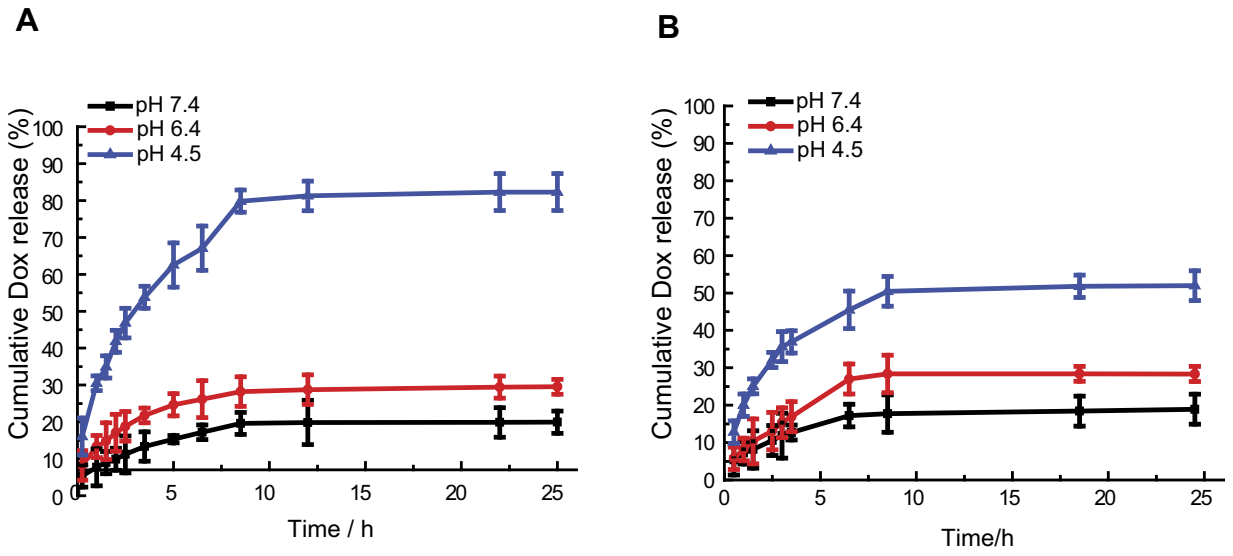

Figure 4 In vitro drug release behavior of MSN-BM/CD-HApt@DOX created via two MSN-BM synthetic pathways at neutral (PBS, pH 7.4) and acidic (PBS, pH 6.4 and 4.5) conditions at 37 °C. In Path I (**A**), the template was removed and then benzimidazole was modified. The BM existed both in porous channels and on the surface of MSN; in path II (**B**), benzimidazole was modified, then the template was removed. The BM only existed on the surface of MSN. The pH-dependent release rates of DOX from MSN-BM/CD-HApt@DOX produced by both pathways were quantified via fluorescence spectrophotometry. The nanoparticle concentration was 100 μg/mL, equivalent to 3.6 μg/mL DOX for Path I and 2.6 μg/mL DOX for Path II. Data are mean ± SD (*n*= 3).

Abbreviations: MSN, mesoporous silica nanoparticles; BM, benzimidazole; CD, β-cyclodextrin; HApt, aptamer; DOX, doxorubicin.

Based on these results, MSN-BM/CD-HApt@DOX prepared by synthetic pathway I was selected for subsequent studies.

MSN-BM/CD-HApt@DOX are specifically taken-up and undergo endocytosis in HER2-positive cells

To investigate the role of HApt on targeted cellular uptake and endocytosis of MSN-BM/CD-HApt@DOX, we used SKBR3 breast cancer cells as a cellular model of HER2 overexpression and MCF7 cells as a model of low HER2 expression; the two cell lines were verified and used in our previous work.[43] Endocytosis of MSN-BM/CD-HApt@DOX was evaluated using confocal laser scanning microscopy (CLSM) and flow cytometry. MSN-BM/CD-NCApt@DOX containing a scrambled nucleotide sequence was used as a control to confirm the specific interaction between HApt and HER2.

CLSM images confirmed MSN-BM/CD-HApt@DOX (relative DOX concentration, 3.6 μg/mL) was specifically taken up by SKBR3 cells (Figure 5B) compared to MCF7 cells (Figure 5A). Stronger red DOX fluorescence was distributed throughout the cytoplasm of SKBR3 cells, indicating the HER2 peptide mediated efficient, specific delivery of MSN-BM/CD-HApt@DOX into SKBR3 cells. Pretreatment with 1.0 μM free HApt significantly decreased the uptake efficiency of MSN-BM/CD-HApt@DOX in SKBR3 cells (Figure 5C), Pre-incubation with HApt had no apparent effect on the uptake of MSN-BM/CD-NCApt@DOX by SKBR3 cells (Figure 6C). These results indicate that the uptake of MSN-BM/CD-HApt @DOX was dependent on the HApt-HER2 interaction.

Quantitative uptake efficiency data was obtained using flow cytometry (Figure 5D and E). MSN-BM/CD-HApt @DOX showed the highest uptake rate in SKBR3 cells (82.7%, IV), further confirming the importance of the interaction between HApt and the HER2 receptor. The uptake rates were much lower in low-HER2 expressing MCF7 cells and SKBR3 cells co-incubated with free HApt as a competitor for the HER2 binding sites (Figure 5D, 31.0% and 40.6%). As nanoparticles up to several hundred nanometers in size can enter cells via endocytosis in membrane-bound vesicles,[50–52] a certain amount of MSN-BM/CD-HApt@DOX or MSN-BM/CD-NCApt@DOX are likely to have been taken up by MCF7 and SKBR3 cells via HER2-independent endocytosis.

Very low DOX fluorescence was observed when MCF7 cells were incubated with MSN-BM/CD-NCApt@DOX (Figure 6A) or SKBR3 cells were incubated with MSN-BM /CD-NCApt@DOX in the absence (Figure 6B) or presence (Figure 6C) of free HApt. These observations further confirmed that the interaction between HER2 and HAPt was required for uptake of MSN-BM/CD-HApt@DOX. The quantitative uptake assays (Figure 6D and E) further confirmed the lack of a specific interaction between NCApt and HER2.

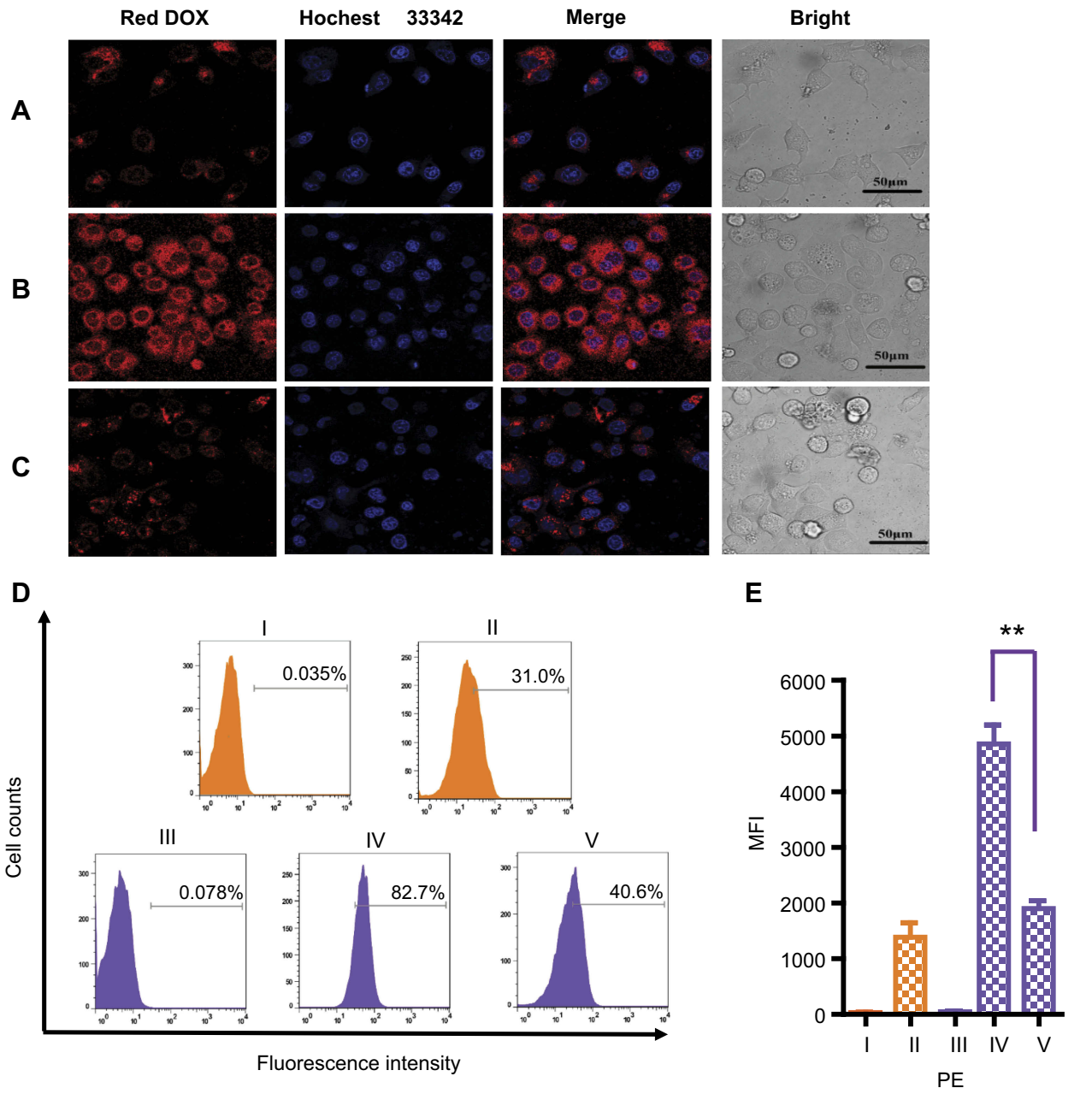

Figure 5 CLSM images of MCF7 (**A**) and SKBR3 (**B**) cells incubated with MSN-BM/CD-HApt@DOX (relative DOX concentration, 3.6 μg/mL) for 4 h. (**C**) CLSM images of SKBR3 cells pretreated with free HApt (1 μM) for 30 min and then co-incubated with MSN-BM/CD-HApt@ DOX (relative DOX concentration, 3.6 μg/mL) for 4 h. Flow cytometric analysis (**D**) and mean fluorescence intensity (MFI, **E**) of MCF7 cells (I and II, orange) incubated with MSN-BM/CD-HApt@DOX (relative DOX concentration, 3.6 μg/mL) for 4 h (II). SKBR3 cells (III, IV and V, purple) incubated with MSN-BM/CD-HApt@DOX (relative DOX concentration, 3.6 μg/mL) in the absence (IV) or presence (V) of free HApt (1 μM) for 4 h. I and III are the corresponding untreated MCF7 and SKBR3 cells. DOX is shown in red; nuclei are stained with Hochest 33,342 (blue). All scale bars are 50 μm. MFI was measured from three independent experiments (n=3). Data are mean ± SD (*n* =3), $^{**}P<0.01$ is considered statistically significant.
Abbreviations: MSN, mesoporous silica nanoparticles; BM, benzimidazole; CD, β-cyclodextrin; HApt, aptamer; DOX, doxorubicin.

Specific cytotoxic effect of HApt in HER2-overexpressing cells

Unloaded nanoparticles

To evaluate the cytotoxicity of the unloaded nanoparticles, HER2-overexpressing SKBR3 HER2-negative MCF7 and normal HEK-293T cells were treated with various concentrations (10–500 μg/mL) of MSN-BM/CD-HApt, MSN-BM/CD-NCApt or MSN-BM/CD and cell viability was assessed using the CCK-8 assay. No significant cytotoxicity was observed in either SKBR3 or HEK-293T cells treated with MSN-BM/CD-NCApt or MSN-BM/CD (Figure 7A and C), even at a high particle concentration of

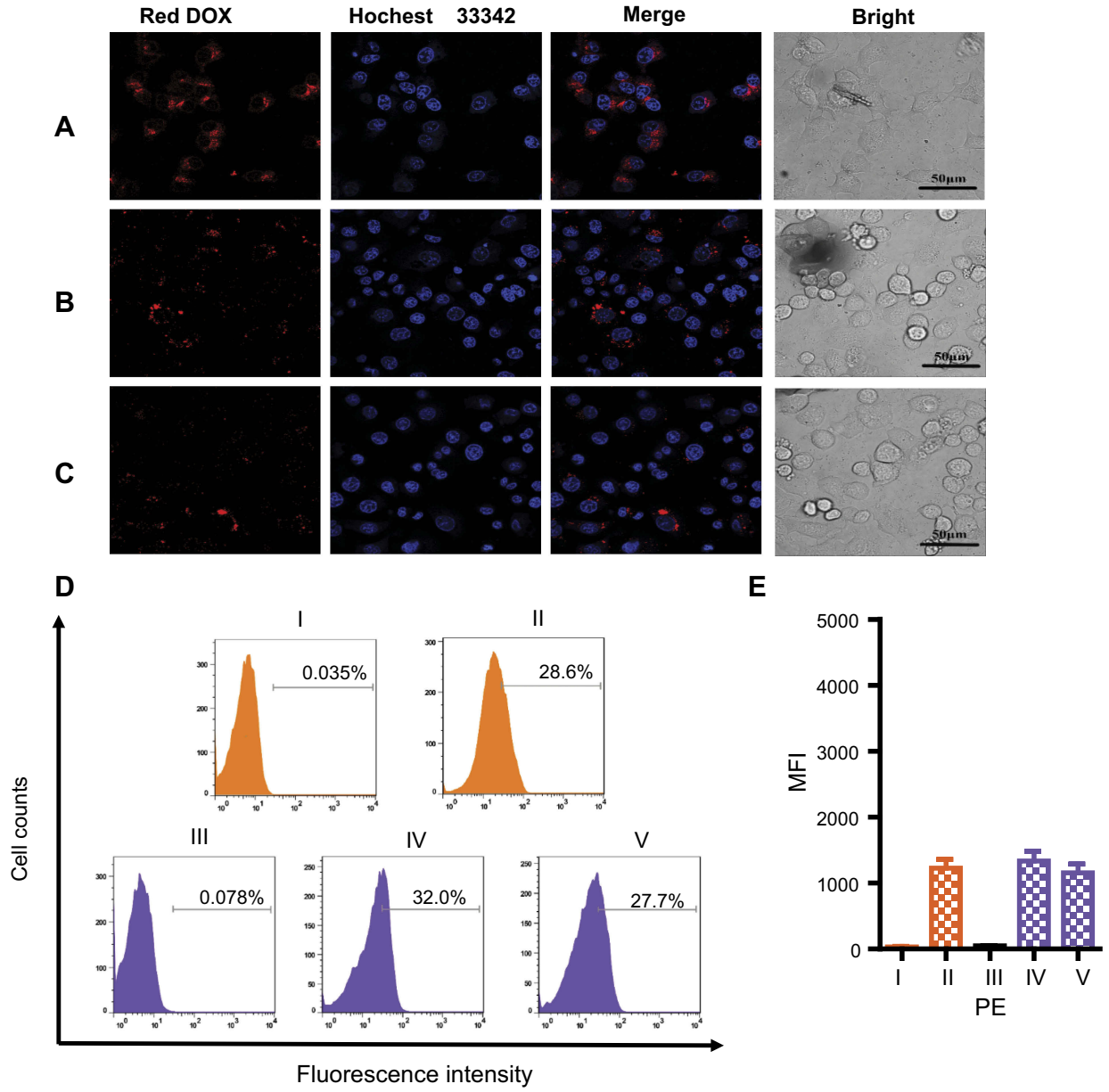

Figure 6 CLSM images of MCF7 (**A**) and SKBR3 (**B**) cells incubated with MSN-BM/CD-NCApt@DOX (relative DOX concentration, 3.6 μg/mL) for 4 h. (**C**) CLSM images of SKBR3 cells pretreated with free HApt (1 μM) for 30 min and then co-incubated with MSN-BM/CD-NCApt@DOX (relative DOX concentration, 3.6 μg/mL) for 4 h. Flow cytometry analysis (**D**) and mean fluorescence intensity (MFI, **E**) of MCF7 cells (I and II, orange) incubated with MSN-BM/CD-NCApt@DOX (relative DOX concentration, 3.6 μg/mL) for 4 h (II). SKBR3 cells (III, IV and V, purple) incubated with MSN-BM/CD-NCApt@DOX (relative DOX concentration, 3.6 μg/mL) in the absence (IV) or presence (V) of free HApt (1 μM) for 4 h. I and III are the corresponding untreated MCF7 and SKBR3 cells. DOX is shown in red; nuclei are stained with Hoechst 33342 (blue). All scale bars are 50 μm. MFI was measured from three independent experiments (n=3). Data are mean ± SD (*n* = 3).
Abbreviations: MSN, mesoporous silica nanoparticles; BM, benzimidazole; CD, β-cyclodextrin; HApt, aptamer; DOX, doxorubicin.

500 μg/mL, demonstrating MSN-BM exhibit good biocompatibility. However, at the same particle concentration, MSN-BM/CD-HApt exerted higher cytotoxicity towards SKBR3 cells than MCF7 cells or normal HEK-293T cells (Figure 7). At a particle concentration of 500 μg/mL, about 55% of HER2-overexpressing SKBR3 cells were killed when incubated with MSN-BM/CD-HApt (Figure 7A), compared to fewer than 5% of MCF7 cells (cell viability: 104.8±4%, Figure 7B) or HEK-293T cells (cell viability: 99.7±3%, Figure 7C), suggesting that MSN-BM/CD-HApt exerts potent cytotoxicity in HER2-overexpressing cells due to HApt-mediated targeting and HER2 downregulation induced cell death.[42] These results indicate MSN-BM/CD-HApt nanoparticles exert toxic effects in HER2 overexpressing cells and imply that the cytotoxicity of these nanoparticles could be increased by DOX loading.

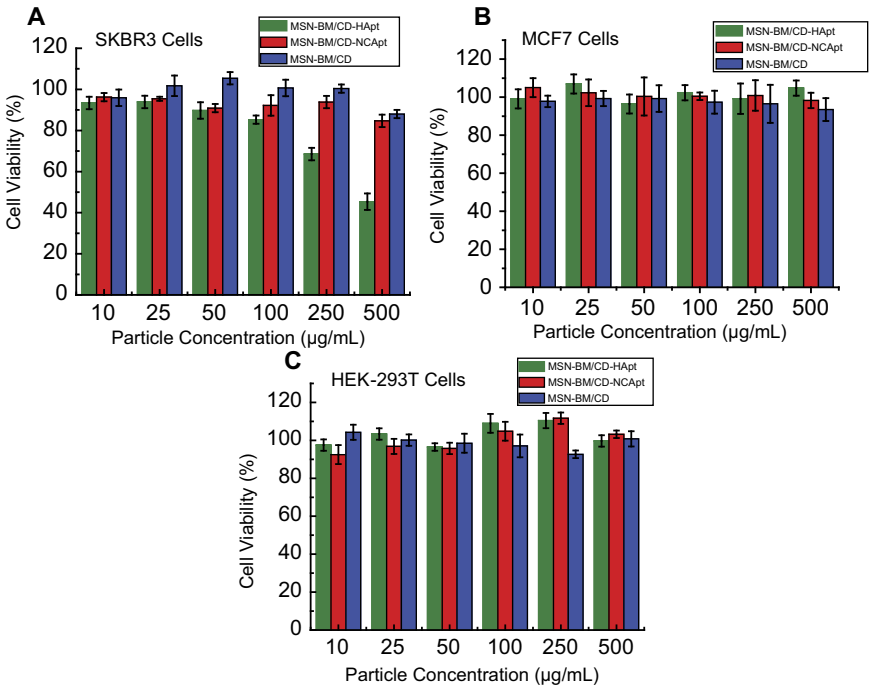

Figure 7 Cell viability of SKBR3 (**A**), MCF7 (**B**) and HEK-293T (**C**) cells incubated with unloaded MSN-BM/CD-HApt, MSN-BM/CD-NCApt or MSN-BM/CD. Cells were incubated with various concentrations of unloaded nanoparticles (10 to 500 μg/mL) for 4 h, then the media was replaced by fresh complete medium and incubated for another 20 h. Cell viability was measured using the Cell Counting Kit-8 (CCK-8). Data are mean ± SD (n = 5).
Abbreviations: MSN, mesoporous silica nanoparticles; BM, benzimidazole; CD, β-cyclodextrin; HApt, aptamer; DOX, doxorubicin.

DOX-loaded nanoparticles

MSN-BM/CD-HApt@DOX was more cytotoxic towards SKBR3 cells than MCF7 cells at the same DOX concentration (Figure 8A); the IC_{50} values of MSN-BM/CD-HApt@DOX in SKBR3 cells and MCF7 cells were about 1.8 μg/mL and 5.5 μg/mL respectively. Moreover, co-incubation with free HApt significantly reduced the cytotoxicity of MSN-BM/CD-HApt@DOX in SKBR3 cells. The Results indicated that the cytotoxic effects of MSN-BM/CD-HApt@DOX were partly mediated by selective, targeted uptake of HApt via HER2. Meanwhile, the mortality of MCF7 and HER2 receptor-shielded SKBR3 cells was not negligible. It was because the MSN- BM/CD-HApt@DOX can also be uptaken partly by cells via the HER2-independent endocytosis (Figure 8A).[52] Then the encapsulated DOX will release in the acidic environment of cellular lysosomes/endosomes and exert cytotoxicity. Furthermore, since the binding between the aptamer and receptor is reversible,[53] free HApt would be replaced partly by MSN-BM/CD-HApt@DOX with increasing concentration, which may resulting in higher cytotoxity. In contrast, the control MSN-BM/CD-NCApt@DOX was less cytotoxic to SKBR3 cells than MSN-BM/CD-HApt@DOX. The presence of free HApt had little effect on the viability of cells incubated with MSN-BM/CD-NCApt@DOX (Figure 8B), as NCApt does not specifically target or exert a selective therapeutic effect in HER2-overexpressing tumor cells. These results further indicate that the cytotoxic effects of DOX-loaded MSN-BM/CD-HApt in HER2-overexpressing SKBR3 cells were partially mediated by the HApt-HER2 interaction.

Synergistic therapeutic effect of MSN-BM/CD-HApt@DOX in HER2-overexpressing cells

Finally, we assessed the combined therapeutic effect of HApt-DOX in HER2-overexpressing SKBR3 cells. Direct exposure to MSN-BM/CD-HApt without loaded DOX (nanoparticle concentration 100 μg/mL) reduced cell viability by about 15 ±2% (Figure 9), while incubation with free DOX or MSN-BM /CD@DOX (DOX concentration, 3.6 μg/mL) decreased cell viability by about 8±4% and 27±6%, respectively. The low cytotoxicity of free hydrophobic DOX (DOX in free base form) may be due to its poor solubility and uncharged properties in aqueous cell medium, which may not conducive to the access and penetration of DOX into cells.[54] In contrast, treatment with MSN-BM/CD-HApt@DOX decreased the viability of SKBR3 cell by about 68±6%, indicating MSN-BM/CD-HApt@DOX exerted a synergistic cytotoxic effect in HER-2

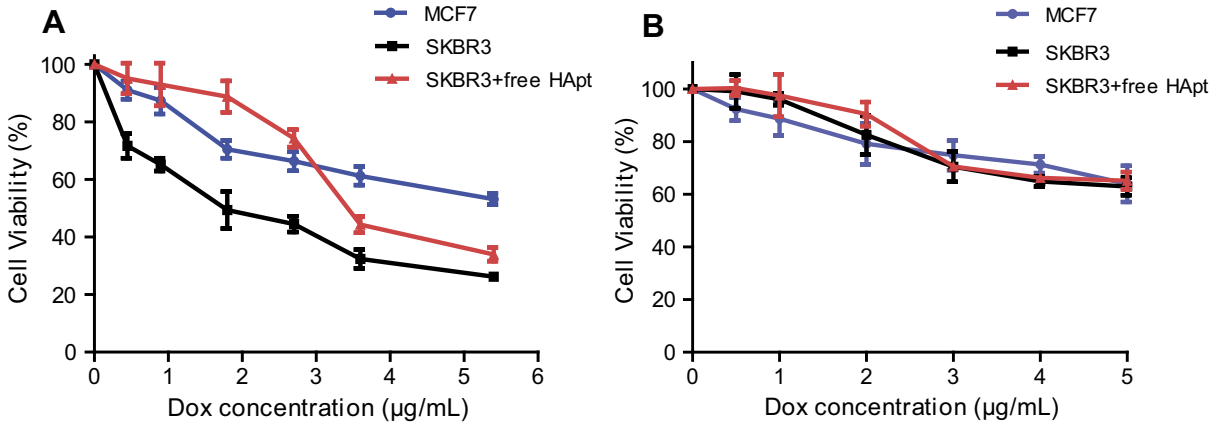

Figure 8 Cell viability of MCF7 and SKBR3 cells incubated with MSN-BM/CD-HApt@DOX (**A**) or MSN-BM/CD-NCApt@DOX (**B**) in the absence/presence of free HApt (1 μM) for 24 h. Cells were incubated with various concentrations of MSN-BM/CD-HApt@DOX or MSN-BM/CD-NCApt@DOX for 4 h, and then with fresh complete media for 20 h. To assay HER2 receptor inhibition, cells were pretreated with free HApt (1 μM) for 30 min, co-incubated with MSN-BM/CD-HApt@DOX or MSN-BM/CD-NCApt@DOX for 4 h, and then cultured in fresh complete media for 20 h. Cell viability was measured using the CCK-8 assay. Data are mean ± SD (n = 5).
Abbreviations: MSN, mesoporous silica nanoparticles; BM, benzimidazole; CD, β-cyclodextrin; HApt, aptamer; DOX, doxorubicin.

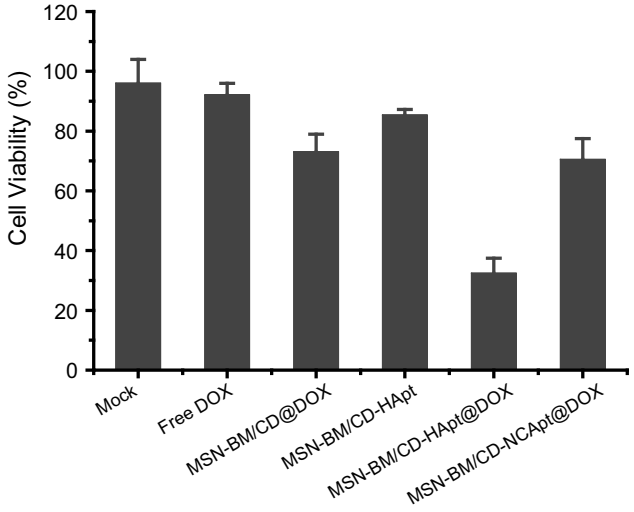

Figure 9 Combined therapeutic effect of MSN-BM/CD-HApt@DOX. SKBR3 cells were exposed to cell culture media (Mock) or cell culture media containing free DOX, MSN-BM/CD@DOX, MSN-BM/CD-HApt, MSN-BM/CD-HApt@DOX or MSN-BM/CD-NCApt@DOX (nanoparticle concentration, 100 μg/mL; DOX concentration, 3.6 μg/mL) for 4 h, and then cultured in fresh complete media for 20 h. Cell viability was measured using the CCK-8 assay. Data are mean ± SD (n = 3).
Abbreviations: MSN, mesoporous silica nanoparticles; BM, benzimidazole; CD, β-cyclodextrin; HApt, aptamer; DOX, doxorubicin.

overexpressing SKBR3 cells. This superadditive effect is mainly due to the specific targeting of HApt, which increased the cellular uptake of MSN-BM/CD-HApt@DOX, allowing a larger number of DOX to be delivered into SKBR3 cells than MSN-BM/CD@DOX.

Conclusion

We successfully developed a HER2-targeted and pH-responsive controlled release system, based on a host-guest interaction between HApt functionalized β-CD and the BM-modified surface of MSN (MSN-BM), to improve the cytotoxic efficiency of the chemotherapeutic agent DOX and biotherapeutic agent HApt in HER2-positive breast cancer cells. Aberrant upregulation of HER2 is observed in around 30% of breast cancers and overexpression of HER2 is associated with the initiation, progression and outcome of breast cancer.[45,55] HApt acted as both a targeting and biotherapeutic agent, which enabled selective delivery and uptake of DOX-loaded nanoparticles by HER2-positive cells. Capping the MSN with CD-HApt reduced the release of DOX at physiological pH (7.4) and conferred stimuli-responsive drug release behavior at acidic pH. In vitro cytotoxicity assays demonstrated MSN-BM/CD-HApt@DOX was efficiently internalized via HER2 receptor-mediated endocytosis, and DOX and HApt exhibited a targeted, synergistic cytotoxic effect in HER2-overexpressing SKBR3 cells. This novel multifunctional nanocarrier may provide new insight into the design, preparation and application of selective, more effective drug delivery systems for HER2-positive breast cancer.

Acknowledgments

Financial support for this work was provided by the National Natural Science Foundation of China (No. 21776071 and No. 31400123), the National Natural Science Foundation of China for Innovative Research Groups (No.51621002), and Research Funds from Shanghai Municipal Commission of Health and Family Planning (No. 201440567).

Disclosure

The authors report no conflicts of interest in this work.

References

1. Cheng YJ, Zhang AQ, Hu JJ, He F, Zeng X, Zhang XZ. Multifunctional peptide-amphiphile end-capped mesoporous silica nanoparticles for tumor targeting drug delivery. *ACS Appl Mater Interfaces*. 2017;9(3):2093–2103. doi:10.1021/acsami.6b12647
2. Yi S, Zheng J, Lv P, et al. Controlled drug release from cyclodextrin-gated mesoporous silica nanoparticles based on switchable host-guest interactions. *Bioconjug Chem*. 2018;29(9):2884–2891.
3. Lu ZR, Qiao P. Drug delivery in cancer therapy, quo vadis? *Mol Pharm*. 2018;15(9):3603–3616.
4. Palanikumar L, Kim J, Oh JY, et al. Hyaluronic acid-modified polymeric gatekeepers on biodegradable mesoporous silica nanoparticles for targeted cancer therapy. *Acs Biomater Sci Eng*. 2018;4(5):1716–1722.
5. Llopis-Lorente A, de Luis B, García-Fernández A, et al. Hybrid mesoporous nanocarriers act by processing logic tasks: toward the design of nanobots capable of reading information from the environment. *ACS Appl Mater Interfaces*. 2018;10(31):26494–26500.
6. Hao WJ, Shen YX, Liu DY, et al. Dual-pH-sensitivity and tumour targeting core-shell particles for intracellular drug delivery. *RSC Adv*. 2017;7(2):851–860.
7. Aznar E, Oroval M, Pascual L, Murguía JR, Martínez-Máñez R, Sancenón F. Gated materials for on-command release of guest molecules. *Chem Rev*. 2016;116(2):561–718.
8. Knežević NŽ, Lin VS. A magnetic mesoporous silica nanoparticle-based drug delivery system for photosensitive cooperative treatment of cancer with a mesopore-capping agent and mesopore-loaded drug. *Nanoscale*. 2013;5(4):1544–1551.
9. Li Y, Duo YH, Bao SY, et al. EpCAM aptamer-functionalized polydopamine-coated mesoporous silica nanoparticles loaded with DM1 for targeted therapy in colorectal cancer. *Int J Nanomedicine*. 2017;12:6239–6257.
10. Louguet S, Rousseau B, Epherre R, et al. Thermoresponsive polymer brush-functionalized magnetic manganite nanoparticles for remotely triggered drug release. *Polym Chem*. 2012;3(6):1408–1417. doi:10.1039/c2py20089a
11. Meng H, Wang MY, Liu HY, et al. Use of a lipid-coated mesoporous silica nanoparticle platform for synergistic gemcitabine and paclitaxel delivery to human pancreatic cancer in mice (vol 9, pg 3540, 2015). *ACS Nano*. 2016;10(6):6416. doi:10.1021/acsnano.6b03110
12. Chen X, Sun H, Hu J, Han X, Liu H, Hu Y. Transferrin gated mesoporous silica nanoparticles for redox-responsive and targeted drug delivery. *Colloids Surf B Biointerfaces*. 2017;152:77. doi:10.1016/j.colsurfb.2017.01.010
13. Choi YL, Ji HL, Jaworski J, Jung JH. Mesoporous silica nanoparticles functionalized with a thymidine derivative for controlled release. *J Mater Chem*. 2012;22(19):9455–9457. doi:10.1039/c2jm30995e
14. Aznar E, Villalonga R, Giménez C, et al. Glucose-triggered release using enzyme-gated mesoporous silica nanoparticles. *Chem commun*. 2013;49(57):6391. doi:10.1039/c3cc42210k
15. Yan H, Teh C, Sreejith S, et al. Functional mesoporous silica nanoparticles for photothermal-controlled drug delivery in vivo. *Angewandte Chemie Inter Ed*. 2012;51(33):8373–8377. doi:10.1002/anie.201203993
16. Hu C, West KR, Scherman OA. Hollow mesoporous raspberry-like colloids with removable caps as photoresponsive nanocontainers. *Nanoscale*. 2016;8(15):7840–7844. doi:10.1039/c6nr01016d
17. Schmidt B, Barner-Kowollik C. Dynamic macromolecular material design-the versatility of cyclodextrin-based host-guest chemistry. *Angewandte Chemie-Inter Ed*. 2017;56(29):8350–8369. doi:10.1002/anie.201612150
18. Qu HN, Yang LR, Yu JM, et al. A redox responsive controlled release system using mesoporous silica nanoparticles capped with Au nanoparticles. *RSC Adv*. 2017;7(57):35704–35710. doi:10.1039/C7RA04444E
19. Llopis-Lorente A, Diez P, de la Torre C, et al. Enzyme-controlled nanodevice for acetylcholine-triggered cargo delivery based on Janus Au-mesoporous silica nanoparticles. *Chem a Eur J*. 2017;23(18):4276–4281. doi:10.1002/chem.201700603
20. Pourjavadi A, Tehrani ZM. Poly(N-isopropylacrylamide)-coated -cyclodextrin-capped magnetic mesoporous silica nanoparticles exhibiting thermal and pH dual response for triggered anticancer drug delivery. *Int J Polym Mater Polym Biomater*. 2017;66(7):336–348. doi:10.1080/00914037.2016.1217531
21. Wang DS, Wu S. Red-light-responsive supramolecular valves for photocontrolled drug release from mesoporous nanoparticles. *Langmuir*. 2016;32(2):632–636. doi:10.1021/acs.langmuir.5b04399
22. Yu JM, Qu HN, Dong TT, Rong M, Yang LR, Liu HZ. A reversible light-responsive assembly system based on host-guest interaction for controlled release. *New J Chem*. 2018;42(8):6532–6537. doi:10.1039/C8NJ00014J
23. Ma HM, Wang YG, Wu D, et al. A novel controlled release immunosensor based on benzimidazole functionalized SiO_2 and cyclodextrin functionalized gold. *Scientific Reports*. 2016;6:19797.
24. Li Q-L, Wang D, Cui Y, et al. AIEgen-functionalized mesoporous silica gated by cyclodextrin-modified CuS for cell imaging and chemo-photothermal cancer therapy. *ACS Appl Mater Interfaces*. 2018;10(15):12155–12163. doi:10.1021/acsami.7b14566
25. Meng HA, Xue M, Xia TA, et al. Autonomous in vitro anticancer drug release from mesoporous silica nanoparticles by pH-sensitive nanovalves. *J Am Chem Soc*. 2010;132(36):12690–12697. doi:10.1021/ja104501a
26. Zhang Z, Ding J, Chen X, et al. Intracellular pH-sensitive supramolecular amphiphiles based on host–guest recognition between benzimidazole and β-cyclodextrin as potential drug delivery vehicles. *Polym Chem*. 2013;4(11):3265. doi:10.1039/c3py00141e
27. Li Z, Clemens DL, Lee B-Y, Dillon BJ, Horwitz MA, Zink JI. Mesoporous silica nanoparticles with pH-sensitive nanovalves for delivery of moxifloxacin provide improved treatment of lethal pneumonic tularemia. *ACS Nano*. 2015;9(11):10778–10789. doi:10.1021/acsnano.5b04306
28. Zhang Y, Chang YQ, Han L, et al. Aptamer-anchored di-polymer shell-capped mesoporous carbon as a drug carrier for bi-trigger targeted drug delivery. *J Mater Chem B*. 2017;5(33):6882–6889. doi:10.1039/C7TB01528C
29. Chen ZH, Sun M, Luo F, Xu KF, Lin ZY, Zhang L. Stimulus-response click chemistry based aptamer-functionalized mesoporous silica nanoparticles for fluorescence detection of thrombin. *Talanta*. 2018;178:563–568. doi:10.1016/j.talanta.2017.09.043
30. Jia X, Wang W, Han Q, Wang Z, Jia Y, Hu Z. Micromixer based preparation of functionalized liposomes and targeting drug delivery. *ACS Med Chem Lett*. 2016;7(4):429–434.
31. Zhang J, Yuan ZF, Wang Y, et al. Multifunctional envelope-type mesoporous silica nanoparticles for tumor-triggered targeting drug delivery. *J Am Chem Soc*. 2013;135(13):5068–5073.
32. Zhang Y, Jiang S, Zhang D, Bai X, Hecht SM, Chen S. DNA-affibody nanoparticles for inhibiting breast cancer cells overexpressing HER2. *Chem commun*. 2017;53(3):573–576.
33. Shao FY, Zhang LH, Jiao L, et al. Enzyme-free immunosorbent assay of prostate specific antigen amplified by releasing pH indicator molecules entrapped in mesoporous silica nanoparticles. *Anal Chem*. 2018;90(14):8673–8679.
34. Jiang F, Liu BA, Lu J, et al. Progress and challenges in developing aptamer-functionalized targeted drug delivery systems. *Int J Mol Sci*. 2015;16(10):23784–23822.

35. Lassalle HP, Marchal S, Guillemin F, Reinhard A, Bezdetnaya L. Aptamers as remarkable diagnostic and therapeutic agents in cancer treatment. *Curr Drug Metab*. 2012;13(8):1130–1144.
36. Zhou ZZ, Liu MY, Jiang JH. The potential of aptamers for cancer research. *Anal Biochem*. 2018;549:91–95.
37. Zhu J, Huang H, Dong SW, Ge L, Zhang Y. Progress in aptamer-mediated drug delivery vehicles for cancer targeting and its implications in addressing chemotherapeutic challenges. *Theranostics*. 2014;4(9):931–944.
38. Zhao F, Zhou J, Su X, et al. A smart responsive dual aptamers-targeted bubble-generating nanosystem for cancer triplex therapy and ultrasound imaging. *Small*. 2017;13(20):16039.
39. Li FQ, Mei H, Xie XD, et al. Aptamer-conjugated chitosan-anchored liposomal complexes for targeted delivery of erlotinib to EGFR-mutated lung cancer cells. *Aaps J*. 2017;19(3):814–826.
40. Ribes A, Aznar E, Bernardos A, et al. Fluorogenic sensing of carcinogenic bisphenol a using aptamer-capped mesoporous silica nanoparticles. *Chem a Eur J*. 2017;23(36):8581–8584.
41. Wang K, Yao H, Meng Y, Wang Y, Yan X, Huang R. Specific aptamer-conjugated mesoporous silica-carbon nanoparticles for HER2-targeted chemo-photothermal combined therapy. *Acta Biomater*. 2015;16:196–205.
42. Lee H, Dam DHM, Ha JW, Yue J, Odom TW. Enhanced human epidermal growth factor receptor 2 degradation in breast cancer cells by lysosome-targeting gold nanoconstructs. *ACS Nano*. 2015;9(10):9859–9867.
43. Shen Y, Zhang J, Hao W, et al. Copolymer micelles function as pH-responsive nanocarriers to enhance the cytotoxicity of a HER2 aptamer in HER2-positive breast cancer cells. *Int J Nanomedicine*. 2018;13:537–553.
44. Yang HL, Lin RW, Rajendran P, et al. Antrodia salmonea-induced oxidative stress abrogates HER-2 signaling cascade and enhanced apoptosis in ovarian carcinoma cells. *J Cell Physiol*. 2019;234(3):3029–3042.
45. Xue L, Maihle NJ, Yu X, Tang SC, Liu HY. Synergistic Targeting HER2 and EGFR with bivalent aptamer-siRNA chimera efficiently inhibits HER2-positive tumor growth. *Mol Pharm*. 2018;15(11):4801–4813.
46. Hou L, Zheng YZ, Wang YC, et al. Self-regulated carboxyphenylboronic acid-modified mesoporous silica nanoparticles with "touch switch" releasing property for insulin delivery. *ACS Appl Mater Interfaces*. 2018;10(26):21927–21938.
47. Resnier P, Montier T, Mathieu V, Benoit JP, Passirani C. A review of the current status of siRNA nanomedicines in the treatment of cancer. *Biomaterials*. 2013;34(27):6429–6443.
48. Tarn D, Ferris DP, Barnes JC, Ambrogio MW, Stoddart JF, Zink JI. A reversible light-operated nanovalve on mesoporous silica nanoparticles. *Nanoscale*. 2014;6(6):3335–3343.
49. Zhang Y, Ang CY, Li M, et al. Polymer-coated hollow mesoporous silica nanoparticles for triple-responsive drug delivery. *ACS Appl Mater Interfaces*. 2015;7(32):18179–18187.
50. Banizs AB, Huang T, Nakamoto RK, Shi W, He J. Endocytosis pathways of endothelial cell derived exosomes. *Molecular Pharmaceutics*. 2018;15(12):5585–5590.
51. Orellana-Tavra C, Haddad S, Marshall RJ, et al. Tuning the endocytosis mechanism of Zr-based metal-organic frameworks through linker functionalization. *ACS Appl Mater Interfaces*. 2017;9(41):35516–35525.
52. Zhang S, Gao H, Bao G. Physical principles of nanoparticle cellular endocytosis. *ACS Nano*. 2015;9(9):8655–8671.
53. Eissa S, Siaj M, Zourob M. Aptamer-based competitive electrochemical biosensor for brevetoxin-2. *Biosens Bioelectron*. 2015;69:148–154.
54. Nasrollahi F, Varshosaz J, Khodadadi AA, Lim S, Jahanian-Najafabadi A. Targeted delivery of docetaxel by use of transferrin/poly(allylamine hydrochloride)-functionalized graphene oxide nanocarrier. *ACS Appl Mater Interfaces*. 2016;8(21):13282–13293.
55. Kuo HP, Chuang TC, Yeh MH, et al. Growth suppression of HER2-overexpressing breast cancer cells by berberine via modulation of the HER2/PI3K/Akt signaling pathway. *J Agric Food Chem*. 2011;59(15):8216–8224.

Supplementary materials

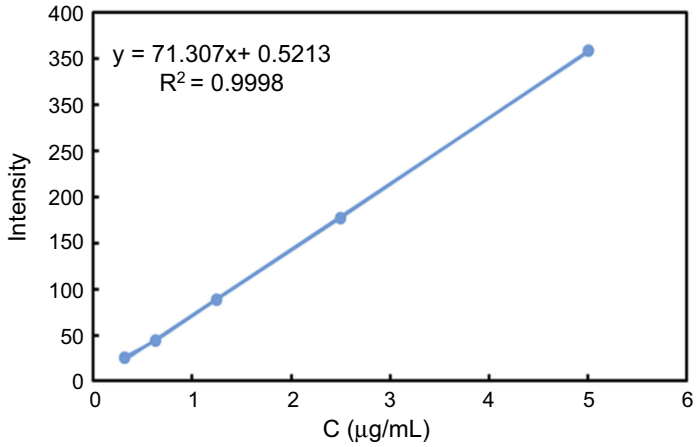

Figure S1 DOX standard curve. A fluorescence spectrophotometer (F-4500; Hitachi, Tokyo, Japan) was used to determine the fluorescence intensity of different concentrations of DOX solution (0.3-5 μg/mL) at an excitation wavelength of 480 nm, emission wavelength of 550 nm.
Abbreviation: DOX, doxorubicin.

Table S1 Properties and parameters of MSN, MSN-BM, MSN-BM/CD and MSN-BM/CD-HApt@DOX

Samples	Diameter (nm)	PDI	ζ-potential (mV)
MSN	176.0±4.2	0.132±0.005	−23.5±7.3
MSN-BM	182.4± 5.0	0.352±0.043	−36.6±4.6
MSN-BM/CD	205.6±3.6	0.246±0.013	−34.3±4.9
MSN-BM/CD-HApt@DOX	218.2± 6.1	0.263±0.014	−31.3±1.4

Notes: Samples were dissolved in PBS (pH 7.4, 1 mM) for size and ζ-potential measurements. Data are mean ± SD (n=5).
Abbreviations: MSN, mesoporous silica nanoparticles; BM, benzimidazole; CD, β-cyclodextrin; HApt, aptamer; DOX, doxorubicin; PBS, phosphate buffered saline.

Table S2 Brunauer–Emmett–Teller and Barrett–Joyner–Halenda measurements for MSN before and after grafting with functional groups

Samples	BET surface area, S_{BET} (m^2/g)	BET pore volume, V_p (cm^3/g)	Pore diameter, D_{BJH} (nm)
MSN	1007.9	0.85	2.59
MSN-BM	797.5	0.53	2.23
MSN-BM/CD-HApt @DOX	238.0	0.11	-

Notes: "–" indicates pores not detected.
Abbreviations: BET, Brunauer–Emmett–Teller; MSN, mesoporous silica nanoparticles; BM, benzimidazole; CD, β-cyclodextrin; HApt, aptamer; DOX, doxorubicin.

Table S3 Brunauer–Emmett–Teller, Barrett–Joyner–Halenda measurements and drug-loading content (DLC) of two MSN-BM synthetic pathways

	BET surface area S_{BET} (m^2/g)	BET pore volume, Vp (cm^3/g)	Pore diameter, D_{BJH} (nm)	Drug loading content (DLC) (±0.3%)
Path Ⅰ	797.5	0.53	2.23	3.64
Path Ⅱ	811.5	0.56	2.34	2.60

Abbreviations: BET, Brunauer–Emmett–Teller; MSN, mesoporous silica nanoparticles; BM, benzimidazole.